THE JOURNAL OF PHYSICAL CHEMISTRY C

Article

pubs.acs.org/JPCC

Binding Specificity of Amino Acids to Amorphous Silica Surfaces: Solid-State NMR of Glycine on SBA-15

Ira Ben Shir, Shifi Kababya, and Asher Schmidt*

Schulich Faculty of Chemistry and Russell Berrie Nanotechnology Institute, Technion - Israel Institute of Technology, Technion City, Haifa 32000, Israel

ABSTRACT: The interactions between bioorganic molecules and inorganic surfaces play a key role in a wide range of multidisciplinary phenomena, among which are catalysis, biomineralization, separation methods, and surface functionalization. Binding of amino acids to inorganic surfaces is of special interest due to their significant role in protein−surface recognition; however, direct experimental evidence on the molecular details of these is scant and often inconclusive. Herein, [1-^{13}C,^{15}N]glycine interactions with amorphous silica surface of SBA-15 were comprehensively characterized using multinuclear, solid-state NMR techniques (REDOR, TEDOR, SLF, 2D-HETCOR). Glycine's ammonium group is shown to interact directly with a specific surface site of a well-defined geometry and stoichiometry: $-NH_3^+$ interacts with 3−4 approximately equidistant (r[N···Si] = 4.1 ± 0.3 Å) silanols, predominantly Q^3's, arranged in a triangular or square geometry (r[Si···Si] ∼ 5 Å). While the $-NH_3^+$ group is surface anchored, the pendent carboxylate reorients with small amplitude with a minor or no contribution to binding. The role of water molecules was studied by increasing surface hydration and temperature and monitoring bound glycine dynamics. Glycine populations with increasing reorientation amplitudes, through isotropic motion of dissolved glycine, coexist, reflecting binding sites solvated by larger water clusters. The similarity of the specific silica site and of the interactions and dynamic modes of bound glycine to those previously reported for L-alanine on SBA-15 suggests we evidence a general binding pattern of amino acids with nonpolar side chains to amorphous silica surfaces. Although loaded from unsaturated aqueous solution, competing with the sparse surface binding, surface-induced crystallization of the α and β polymorphs occurred. Tailored solid-state NMR methodology yields direct, quantitative experimental evidence that enables molecular-functional description of the interfacial interactions and further demonstrates the importance of this class of techniques in the wide field of surface science.

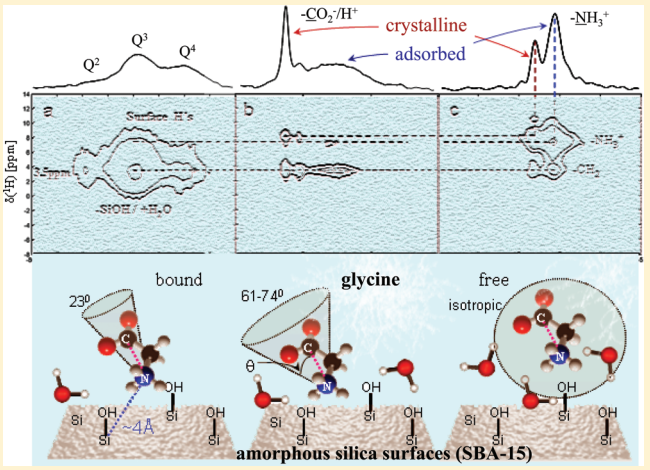

INTRODUCTION

In the past decade, the interactions between bioorganic molecules and inorganic surfaces have drawn a vast interest due to their significant role in a wide range of multidisciplinary topics,[1] including catalysis,[2] biomineralization,[3−5] biosensors,[6] implants,[7] and prebiotic chemistry.[8,9] One class of such systems is the binding of amino acids and peptides to amorphous silica surfaces. Being the most abundant mineral on Earth, silica was extensively studied and employed for a wide range of applications.[10] Few of the diverse usages where silica is a key component span catalysis, chromatography, optoelectronic devices, and solar cells.[11] One source of silica applicability is in the great variety of natural and synthetic silica polymorphs either crystalline or amorphous, glasses or sol−gel phases, which further can form micro- and mesoporous structures.[12] All silicas are three-dimensional networks composed of the common SiO_4 tetrahedra building blocks; the flexibility of the Si−O−Si bond is responsible for the diverse properties of the materials formed. Mesoporous silica materials are a class of synthetic materials with high surface area composed of amorphous silica that is periodic on the mesoscopic length scale.[13] Two well-known examples are MCM-41[14] and SBA-15[15] with pore diameters of 2−4 and 5−30 nm, respectively. The structure of mesoporous silicas has been studied extensively by X-ray[16−18] and neutron diffraction,[17] EPR,[19,20] transmission and scanning electron microscopy,[2] and solid-state NMR,[21,22] making these materials relatively well-defined and thus excellent model surfaces.

Amino acids, which are the simplest biomolecules, serve as the building blocks of peptides and proteins. They play significant role in protein−surface interactions[1] and, moreover, are convenient for functionalization of solid surfaces due to their multifunctionality. Surfaces and adducts exhibit a wide scope of catalytic activity with numerous and diverse applications; also, the reactivity of the amino acids themselves is altered upon binding and under adequate conditions may result in peptide bond formation.[23] Yet, direct experimental

Received: March 13, 2012
Published: April 12, 2012

   dx.doi.org/10.1021/jp302431t | J. Phys. Chem. C 2012, 116, 9691−9702

evidence on the molecular details of their mutual interactions and absorption mechanism is scant and often contradicting.[24] Detailed characterization of the interactions of amino acids with inorganic surfaces would contribute significantly to the understanding of biomolecular adsorption phenomena and enhance the ability to design functional surfaces.

High-resolution solid-state NMR is one of the most insightful techniques for characterization of interfacial interactions between biomolecules and inorganic surfaces.[25−30] Diverse NMR techniques can provide structural and dynamical details at the atomic/molecular level of interfaces, with REDOR (rotational echo double resonance) being a key technique.[31] REDOR NMR, to-date a well-established analytical technique, provides means to directly identify the interacting species of the biomolecule and of the surface, determine intermolecular (interatomic) distances, and the local dynamics.[32−35] Often, to overcome NMR spectroscopy's inherently low sensitivity, stable isotope enrichment of the biomolecules and high surface area inorganic materials are required.

We have recently reported the study of L-[1-^{13}C,^{15}N]alanine loaded onto SBA-15 mesoporous silica employing solid-state NMR.[33] The surface interacting alanine moiety was identified as the $-NH_3^+$ functional group by ^{15}N{^{1}H} separated local field (SLF) NMR. ^{29}Si{^{15}N} and ^{15}N{^{29}Si}REDOR NMR revealed specific intermolecular interactions between $-NH_3^+$ and 3−4 surface Si species, predominantly Q^3, with similar internuclear N···Si distances of 4.0−4.2 Å and Si···Si distances of ∼5.0 Å. ^{15}N{^{13}C}REDOR NMR clearly showed that while alanine is anchored via its $-NH_3^+$, its carboxylate end undergoes small-amplitude motion. Upon increased hydration and temperature, the motional amplitude of this pendent carboxylate grows larger, until onset of dissolution occurs. Furthermore, the coexistence of at least three populations of differently bound alanine molecules was identified (^{15}N{^{13}C}REDOR NMR), indicating both bound and free populations. These distinct populations were attributed to alanine binding at surface sites with water clusters of different sizes.[36,37] Upon increased hydration, surface water clusters grow bigger and are more abundant. The description of alanine binding in which the $-NH_3^+$ group is surface anchored while the carboxylate end undergoes dynamic motion therefore infers that the carboxylate has small or no contribution to surface binding.

The adsorption of the simplest amino acid, glycine, on silica surface was investigated extensively both experimentally and computationally. For example, DFT modeling of microsolvated glycine on an amorphous silica surface predicted opposite binding model to that we observed for L-alanine.[38−40] In this model glycine binds to the geminal hydroxyl groups through its carboxylate functionality and lying parallel to the surface with the $-NH_3^+$ moiety interacting with water molecules with no contribution to binding. Earlier experimental studies suggested that the interacting moiety is the charged $-NH_3^+$ group;[23,41] however, later studies attribute binding to its carboxylate group.[9,42] As yet, the accumulated evidence is insufficient to define how this amino acid interacts with silica surfaces, either directly or indirectly, through the carboxylate or the amine group.[9,42] Moreover, the alluded specificity of the binding site could not be deciphered; hence, the identity of the participating functional groups of the surface, their stoichiometry and local geometry, and the effects of water molecules as they accumulate at the binding site remained open questions. The inconclusiveness of the accumulated computational predictions and experimental studies further triggered our interest in the actual binding mechanism of glycine. In addition, extending our earlier study of alanine adsorption on SBA-15[33] should address the question of whether a general pattern of small amino acid−silica interfacial interactions exists for amino acids with nonpolar side chain. The above issues are fully answered in this article using primarily multinuclear solid-state NMR techniques.

First, we describe the α and β crystalline polymorphs of glycine that coexist with the sparsely adsorbed glycine molecules on the SBA-15 surface. Although glycine was loaded from unsaturated aqueous solution, surface-induced crystallization occurs in parallel to surface binding. This phenomenon has been reported earlier for glycine in contact with amorphous silica surfaces,[42] and here we further substantiate the crystalline characteristics of the glycine polymorphs. Following, we address the nature of glycine−SBA-15 interactions and the identity of the interacting moieties of both glycine and silica as well as the specific binding site—its binding geometry and stoichiometry. We then elucidate the dynamic state of glycine molecules adsorbed onto the silica surface, determine the presence of different populations and their distribution, and the influence of the hydration level and temperature on the binding, as reflected by the motional behavior of the adsorbed amino acids. Finally, using {^{1}H}^{29}Si/^{13}C/^{15}N 2D HETCOR experiments, we resolve and identify the distinct hydrogen environments at both the silica−glycine interface and within each of the crystalline polymorphs of glycine.

Noteworthy, solid-state NMR methodology was already utilized to investigate glycine−silica interface,[9,23,42] and its strength and adequacy for surface science were highlighted. However, as is shown in this work, the solid-state NMR approach is fully exploited only upon devising selective dipolar recoupling/decoupling techniques which directly monitor inter- and intramolecular interactions that so serve as geometric and dynamic probes. These techniques, applied to the specifically labeled ^{13}C and ^{15}N amino acid, enable for the first time a comprehensive description of the mechanism of surface adsorption.

EXPERIMENTAL SECTION

Materials. Specifically labeled compounds with stable isotope enrichment levels of 98% were used as received. [1-^{13}C,^{15}N]Glycine was purchased from CIL, and L-[u-^{15}N,^{13}C]lysine·2HCl was purchased from D-Chem (Israel). SBA-15 (natural abundance ^{29}Si) was the kind gift of Prof. M. Landau, Ben-Gurion University. The SBA-15 was characterized[36] by N_2 adsorption/desorption isotherm measurements with a NOVA-2000 (Quantachrome, version 7.01) apparatus. The surface area of 850 m^2/g, pore volume 11.3 cm^3/g, and pore diameter of 59.1 Å were obtained from the isotherms using the BET and BJH methods. Micropores contribute only 3% to the surface area of the material and are therefore neglected.

Sample Preparation. . Loading of 0.2 [1-^{13}C,^{15}N]glycine molecules/nm^2 on SBA-15 was performed as previously reported by Vega and co-workers.[36] 60 mg of calcined SBA-15, which was initially heated to 180 °C for 3 h (to remove residual water), was added to a 1.5 mL aqueous solution of 48 mg of [1-^{13}C,^{15}N]glycine (0.42 M). The suspension was stirred for 3 h at room temperature. The mixture was then filtered (Nanosep 300k omega), and the remaining powder was allowed to dry in air. The remaining powder was then packed inside 5 or 4 mm zirconia rotors with Teflon plugs and Vespel

dx.doi.org/10.1021/jp302431t | J. Phys. Chem. C 2012, 116, 9691−9702

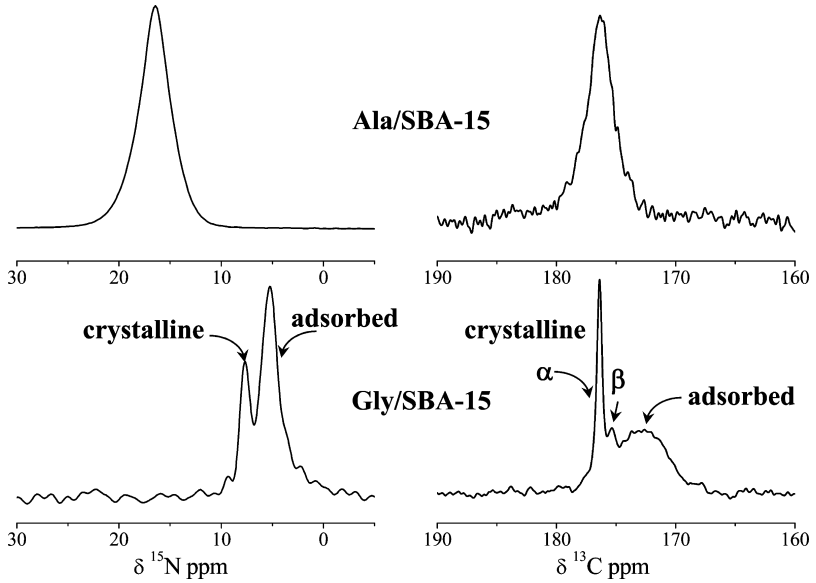

Figure 1. ^{15}N and ^{13}C CPMAS NMR spectra of [1-^{13}C,^{15}N]glycine/SBA-15 at the "intermediate" hydration state (bottom) and of L-[1-^{13}C,^{15}N]alanine/SBA-15 (top).[33]

drive tips. The hydration level was reduced by evacuating the sample (while inside the rotor with cap removed): pumping (10^{-3} Torr) for few hours yielded the "hydrated" state; extended pumping for 7 days yielded the "dry" state. Hydration level was raised by sample exposure to ambient atmosphere for limited time period, which yielded the "intermediate" state. Three hydration states of the sample, denoted "dry", "intermediate", and "hydrated", all representing minute water content, are considered. The water content of the three hydration states range was evaluated by ^{1}H MAS NMR showing between 1 and 6 water molecules per nm^2.[36] We emphasize that the different hydration states and temperatures represent reversible states. The short notation Gly/SBA-15 will be used throughout the to denote the [1-^{13}C,^{15}N]glycine loaded on SBA-15.

Solid-State NMR. NMR spectroscopy measurements were carried out on a Chemagnetics/Varian 300 MHz CMX-infinity solid-state NMR spectrometer equipped with three radio-frequency channels and 5 mm triple-resonance APEX Chemagnetics probe using 5 mm zirconia rotors. Samples were spun at 5000 ± 2 Hz throughout the experiments. Cross-polarization (CP) magic angle spinning (MAS) echo experiments (indirect excitation) were carried out with a 5.0 μs $\pi/2$, 10.0 μs π pulse widths, an echo interval τ (200 μs) identical to the rotor period T_R, a ^{1}H decoupling level of 100 kHz, and a relaxation delay of 1.5 or 2 s; Hartmann–Hahn rf levels were matched at 50 kHz, with contact time of 1 ms for ^{15}N and 1.5 ms for ^{29}Si.

Direct ^{15}N excitation echo experiments (DE) were carried out with 5.0 μs $\pi/2$, 10.0 μs π pulse widths, an echo interval τ equal to the rotor period T_R (200 μs), a ^{1}H decoupling level of 100 kHz, and a relaxation delay of 2 s. $^{15}N\{^{29}Si\}$, $^{29}Si\{^{15}N\}$, and $^{15}N\{^{13}C\}$ REDOR experiments were conducted using a REDOR pulse sequence with refocusing π pulses on each rotor period (T_R) on the observe channel and dephasing π pulses in the middle of each rotor period on the nonobserved nuclei, followed by an additional two rotor periods with a chemical shift echo π pulse in the middle. REDOR π pulses employed xy8 phase cycling for the refocusing and recoupling pulses.[31,43] Data acquisition employed an alternating block scheme, collecting a single S_0 transient with recoupling pulses turned off, followed by S_R transient collection with recoupling pulses turned on. REDOR difference data obtained via $S_0 - S_R$ subtraction, ΔS, yield spectra which exclusively exhibit peaks of dipolar-coupled chemical species. All REDOR data presented in the figures were collected using the CP excitation scheme. A representative set of experimental $^{15}N\{^{29}Si\}$ REDOR data points were also measured for both "dry" and "hydrated" states, employing the DE excitation scheme. The resulting DE-REDOR data (not shown) overlapped with CP-REDOR data, hence confirming that all glycine populations are correctly reported by the CP excitation. The number of collected transients was set to yield adequate signal-to-noise ratio; a typical number of transients are 2048 and 10 240 for experiments detecting ^{15}N and ^{29}Si, respectively.

The chemical shifts of ^{15}N and ^{29}Si are reported relative to $(^{15}NH_4)_2SO_4$ (solid) and TMS, respectively. Simulations and fitting of REDOR data were performed using SpinEvolution.[44] Peak areas were calculated by deconvolution using DMFIT.[45]

The SLF solid-state NMR technique was modified to include the phase modulated Lee–Goldberg (wPMLG5)[46−50] homonuclear decoupling. Specifically, the odd dipolar-rotational spin-echo (ODRSE) experimental scheme of Bork et al. was used.[51] The experimental parameters of the optimized PMLG5 cycle employed on-resonance ^{1}H irradiation with a 1.9 μs pulse width, 90 kHz rf level, 0.1 μs delay for phase setting, and with an overall cycle time of 20 μs. For the simulations 11.4 kHz N–H dipolar coupling (1.01 Å N–H distance) was used, reduced to 3.88 kHz accounting for the internal fast C_3 rotation, and additionally multiplied by the PMLG5 scaling factor of 0.58.

A 500 MHz AVANCE III (Bruker) equipped with triple-resonance probes 4 mm zirconia rotors, spinning at 10 000 ± 2 Hz and 5000 ± 2 Hz, was used for 2D HETCOR.

A 2D-HETCOR $^{13}C\cdots^{15}N$ experiment was run employing 16 × 16T_R $^{13}C \rightarrow {}^{15}N$ TEDOR mixing.[52−55] This experimental scheme starts with CP to ^{13}C (using the same parameters as for the ^{15}N CPMAS spectra, above) followed by a t_1 evolution period in which the isotropic chemical shift of the ^{13}C is encoded; t_1 was incremented 16 times, with Δt = 0.2 ms (=T_R).

dx.doi.org/10.1021/jp302431t | J. Phys. Chem. C 2012, 116, 9691–9702

The subsequent TEDOR mixing is made up of $16T_R$ REDOR dipolar recoupling blocks in the preparation and buildup periods, i.e., before and after the (central) coherence transfer step via the two back-to-back $\pi/2$-pulses (on the ^{15}N- and ^{13}C-nuclei). In the $16T_R$ TEDOR preparation the refocusing π-pulses are on the ^{13}C-channel (recoupling pulses in the middle of each rotor period on the ^{15}N channel), and in the $16T_R$ buildup period they are on the ^{13}C-channel (recoupling pulses on the ^{13}C). Similar to the REDOR sequence above, an additional $2T_R$ period with a π-pulse in the middle is added to form simultaneously a Hahn and a rotational echo.

$^1H\{^{29}Si/^{13}C/^{15}N\}$ HETCOR experiments were run employing wPMLG5 homonuclear decoupling scheme during t_1 ^1H chemical shift evolution period, with 92, 419, and 130 increments (respectively) spaced by 11 μs, followed by CP (using the same parameters as described above) with 4, 0.2, and 0.3 ms contact times and 512, 64, and 64 transients collected for each t_1 increment, respectively.

RESULTS AND DISCUSSION

Surface Adsorption vs Surface-Induced Crystallization of Glycine. In order to introduce the unique characteristics of the [1-^{13}C,^{15}N]glycine-loaded SBA-15 system, we describe first the "intermediate" hydration level. The ^{15}N and ^{13}C CPMAS spectra of [1-^{13}C,^{15}N]glycine/SBA-15 both exhibit two classes of resolved peaks (Figure 1, bottom), broad and narrow, representing distinct types of glycine ammonium and carboxylate. The positions of the narrow and broad peaks in both ^{13}C and ^{15}N glycine spectra (Table 1) are consistent with the literature values of crystalline and surface adsorbed species, respectively.[56] The respective spectra of L-[1-^{13}C,^{15}N]alanine/SBA-15[33] exhibiting only the peaks of the surface adsorbed alanine are shown for comparison in Figure 1, top. The ^{13}C carboxylic and ^{15}N amino chemical shifts are very sensitive to the chemical environment, being affected by both their protonation states, hydrogen bonding, and crystal packing parameters (polymorph).[42,57,58] The higher resolution of the ^{13}C CPMAS spectrum (Figure 1 bottom, right) enables to distinguish the occurrence of the α and β polymorphs of glycine (Table 1).[42,57]

Table 1. Chemical Shifts of the Different Glycine Species

glycine	^1H amino (ppm)	^{13}C carboxylate (ppm)	^{15}N amino (ppm)
crystalline α	2.6, 3.8 (CH_2), 8.0 (NH_3)	176.4	7.7
crystalline β	3.0 (CH_2), 8.0 (NH_3)	175.5	
surface bound	3.0 (CH_2), 7.2 (NH_3)	172.6	4.7−5.4[a]

[a]With increased hydration the chemical shift of the adsorbed peak increases and the heterogeneous peak width (fwhh) decreases: 4.7 ppm ($\delta\nu$ ~4.3 ppm) and 5.4 ppm ($\delta\nu$ ~2.2 ppm) for the "dry" and "hydrated" states, respectively.

As further means to confirm the ^{15}N and ^{13}C assignments, we have carried out a 2D-HETCOR NMR experiment using a 16 × 16 $^{13}C\{^{15}N\}$ TEDOR mixing period. Its resulting spectrum (Figure 2) reveals two distinct carboxylic−amino cross-peaks: an intense one connecting the narrow crystalline species, alongside a weak one connecting the broad, more shielded species of the surface adsorbed glycine molecules. The significantly larger peak width of the adsorbed vs the crystalline glycine peaks reflects the much higher local heterogeneity of molecules adsorbed on the amorphous surface, as opposed to the uniform environments within the molecular crystals. The lower cross-peak intensity of the adsorbed vs the crystalline glycine is apparently in contrast to their higher relative intensities in the respective 1D CPMAS spectra (Figure 1, bottom). In part, this is a result of the dynamics of the adsorbed molecules ("intermediate" hydration state, *vide infra*) that reduces the intramolecular $^{13}C\cdots^{15}N$ dipolar coupling, hence limiting the coherence transfer efficiency in the TEDOR mixing period.

The occurrence of surface-induced crystallization of glycine polymorphs when amorphous silica (Aerosil 380) is loaded from undersaturated solution was reported earlier and characterized by solid-state NMR, showing a similar set of peaks of the coforming crystalline and surface adsorbed species.[42] β-Glycine is thermodynamically metastable;[59] however, both our SBA-15-induced crystals and those reported by Lopes et al.[42] were found stable. Further NMR characterization of the crystalline phases will be presented together with that of the adsorbed molecules.

Characterization of Adsorbed Glycine/SBA-15: "Dry" State. *Interacting Surface Sites.* Characterizing the different chemical structures of the amorphous silica, and in particular the surface species, is achieved using $\{^1H\}^{29}Si$ CPMAS, with a representative spectrum of Gly/SBA-15 at the "dry" state shown in Figure 3 (bottom left). This spectrum shows the typical Q^2 ($Si^*(OSi)_3(OH)_2$), Q^3 ($Si^*(OSi)_3OH$), and Q^4 ($Si^*(OSi)_4$), with Q^3 the strongest peak in accordance with its identification as the primary surface species.[60,61] The cross-polarization ($^1H \rightarrow {}^{29}Si$) selects ^{29}Si moieties proximate to ^1H nuclei and hence emphasizes species present on the SBA-15 silica surface. This CP selection is further emphasized at populated binding sites, where the hydrogen atoms of glycine contribute the major fraction of the proton density (especially at the lowest hydration as of the "dry" state).

Direct observation of which of the Si species in the hydrogen-rich environments interact with the adsorbed glycine is made possible by the REDOR experiments. This spectroscopic technique, taking advantage of the dipolar interaction that occurs between two molecularly proximate species (3−15 Å),[31,62] enables to spectrally edit these of 10 min functional-interacting moieties out of the bulk and also to determine their intermolecular (internuclear) distance. The $^{29}Si\{^{15}N\}$ REDOR difference spectrum, ΔS (Figure 3, top left), of the Gly/SBA-15 ("dry" state) clearly shows peaks primarily for Q^3, therefore demonstrating the proximity of glycine amine to these species. This spectrum is the first direct evidence of this surface−glycine interaction.

Glycine−Ammonium Interaction with the Silica Surface: Geometry and Stoichiometry. This evidence is now further refined and the local geometry determined by switching the REDOR experiment to observe the amine nitrogen. The $128T_R$ $^{15}N\{^{29}Si\}$ REDOR (Figure 3, right top) spectra of the [1-^{13}C,^{15}N]glycine/SBA-15 at the "dry" state show a pronounced REDOR difference peak, ΔS, exclusively for the partially resolved broad ^{15}N component (~5.0 ppm) of the surface adsorbed glycine. This measurable $^{15}N\cdots^{29}Si$ intermolecular dipolar coupling further indicates the occurrence of interactions of adsorbed glycine molecules with the SBA-15 surface via their charged ammonium moiety (*vide infra*), similar to our earlier findings for alanine.[33] The narrow crystalline component is seen intact in the S_R spectrum (Figure 3, right

dx.doi.org/10.1021/jp302431t | J. Phys. Chem. C 2012, 116, 9691−9702

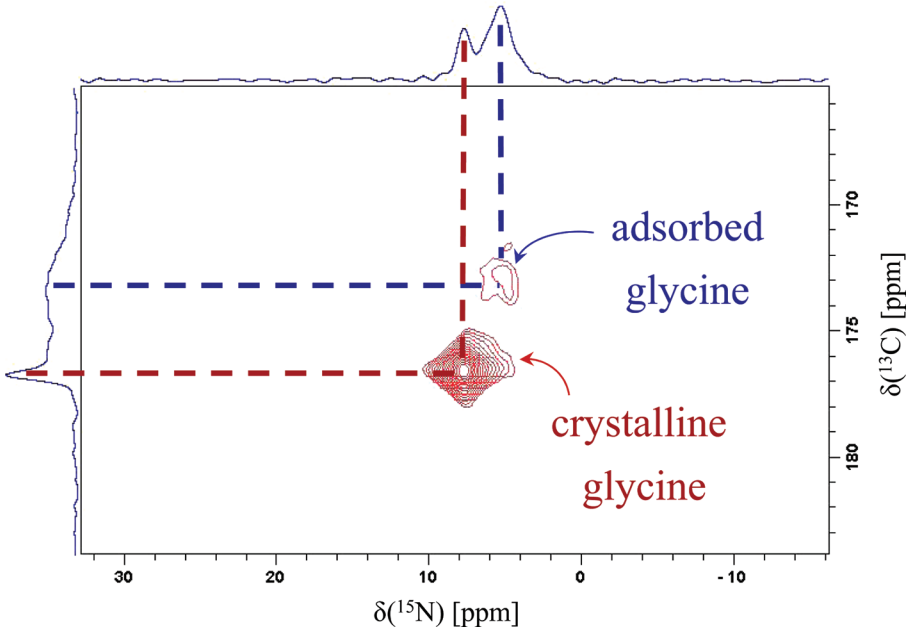

Figure 2. 2D $^{13}C\{^{15}N\}$ HETCOR NMR spectrum of [1-^{13}C,^{15}N]glycine/SBA-15 at the "intermediate" hydration state. A 16 × 16T_R $^{13}C \rightarrow {}^{15}N$ TEDOR mixing period was employed. The 1D spectra are the respective CPMAS spectra shown in Figure 1.

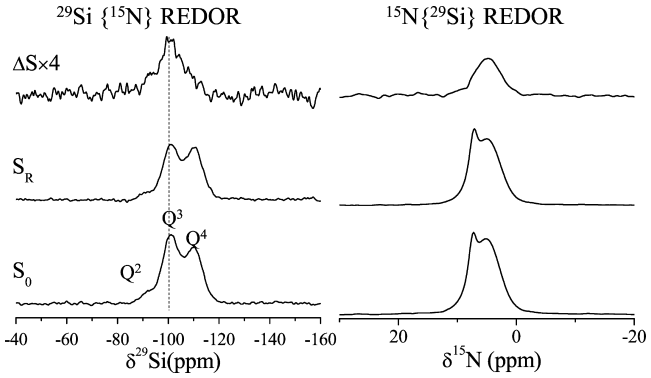

Figure 3. [1-^{13}C,^{15}N]Glycine loaded onto SBA-15 at the "dry" state. Left: $^{29}Si\{^{15}N\}$ 128T_R (25.6 ms) REDOR spectra at −20 °C. Dephasing of the Q^3 species dominates the difference spectra (ΔS, top), identifying it as the preferential surface functional group that binds *N*-ammonium of glycine. Right: $^{15}N\{^{29}Si\}$ 128T_R (25.6 ms) REDOR spectra at 4 °C. The narrow 7.7 ppm peak (~0.7 ppm fwhh) and the broad ~5.0 ppm peak (3.7 ppm fwhh) are assigned to crystalline and adsorbed glycine, respectively. Only the ^{15}N component of the adsorbed glycine at ~5.0 ppm (broad) is attenuated (undergoes dephasing, ΔS, top), while the crystalline component remains intact (S_R, middle).

middle), hence reporting no surface contacts. This distinctions also substantiates the above $^{29}Si\{^{15}N\}$ REDOR findings: detectable Q^3-amine proximities are only due to the adsorbed glycine.

The measured $^{15}N\{^{29}Si\}$ REDOR evolution between 32 and 128T_R shows monotonic decrease of the S_R/S_0 peak (Figure 4) of the adsorbed component, reaching a maximal attenuation of ~11%. In a situation where a glycine nitrogen atom is proximate to a single surface Si atom, the probability of the latter being a ^{29}Si equals its 4.7% natural abundance and so is the maximum REDOR attenuation. The observed ~11% attenuation at the longest measured recoupling time (N = 128, t = 25.6 ms, Figure 4), being greater than the 4.7% natural abundance of ^{29}Si, indicates that the ammonium group must reside closely equidistant to three or more Si atoms when adsorbed.

The crystalline facets of *β*-cristobalite[63] are reported to have surface characteristics close to amorphous silica,[60,64] exhibiting trigonal (111) and square (100) geometries of surface silanol groups, both with shortest Si···Si distances of 5.07 Å (Figure 4, top). These geometries therefore serve as approximated starting models. For a quantitative geometric assessment of glycine on the SBA-15 surface the ammonium group is centered above 3 or 4 surface Si atoms (Figure 4, top), such that the ^{15}N nucleus is at the head of either a trigonal or a square pyramid and equidistant from the Si atoms. Such geometric arrangements may yield maximum possible REDOR attenuation of 14.1% (3 × 4.7) and 18.8% (4 × 4.7), respectively, in a manner previously described also for alanine.[33]

Using the trigonal and square geometric models, the N···Si internuclear distance for isolated $^{15}N\cdots{}^{29}Si$ pairs is determined by fitting the experimental data with simulated REDOR evolution curves.[44] The best fits yield $^{15}N\cdots{}^{29}Si$ dipolar coupling strengths of 38 and 33 Hz (3 and 4 Si neighbors), corresponding to r[N···Si] of 4.0 ± 0.2 and 4.2 ± 0.2 Å, respectively (Figure 4). This tight geometry does not leave room for a water molecule to mediate glycine amine and the binding hydroxyls, hence classifying the interaction as direct. Furthermore, the measured $^{15}N\{^{29}Si\}$ REDOR evolution was found temperature independent between −20 and 20 °C (Figure 4, bottom). This unaffected intermolecular binding (fixed N···$Si_{(n)}$ internuclear distances) implies relatively strong interactions.

The geometric arrangement of the adsorbed glycine molecules on SBA-15 silica surface is found to be very similar to that of adsorbed alanine and similarly temperature insensitive when both are at the dry state.[33]

Protonation State of Amino Group. Although the chemical shift of the ^{15}N-amine group depends on its protonation state (positive vs neutral), it is also sensitive to the immediate chemical environment (crystalline vs adsorbed), and therefore

dx.doi.org/10.1021/jp302431t | J. Phys. Chem. C 2012, 116, 9691−9702

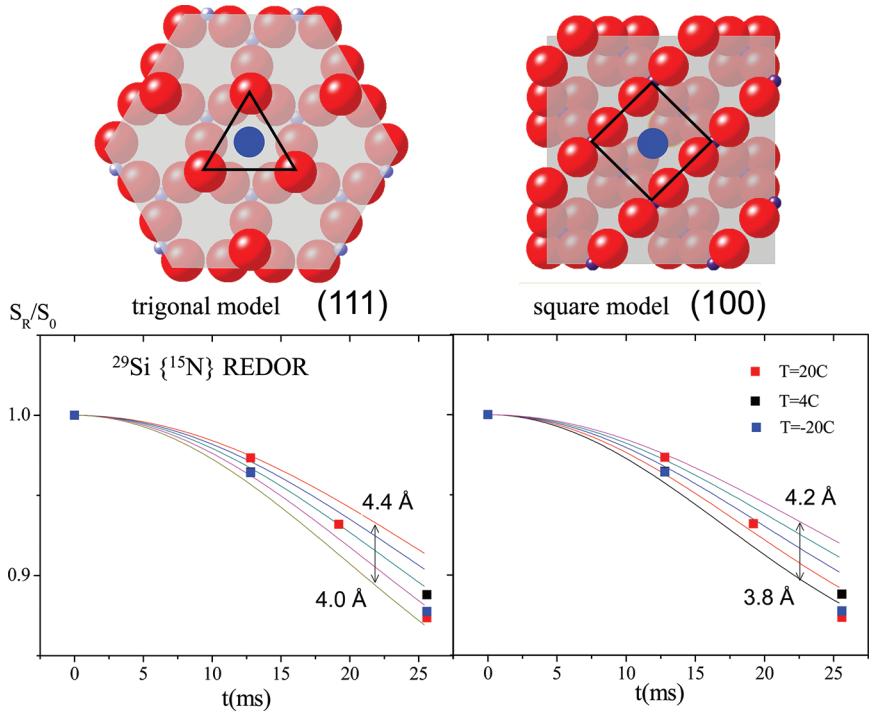

Figure 4. Top : top view of (111) (left) and (100) (right) crystal planes of β-crystobalite with an N atom (blue, representing glycine amine) centered above triangular and square planar arrangements of Si atoms (purple), respectively. A surface silicon atom is present below each corner of the black triangle and square. The red circles represent oxygen atoms. Bottom: experimental $^{15}N\{^{29}Si\}$ REDOR dipolar evolution data of [1-^{13}C,^{15}N]glycine/SBA-15 in the "dry" state at temperatures of −20 and 20 °C. Simulated REDOR curves for different N···Si distances that span the width of the experimental error are normalized to maximum relative attenuations of 14.1 and 18.8% for the triangular (left) and square (right) pyramid models, respectively.

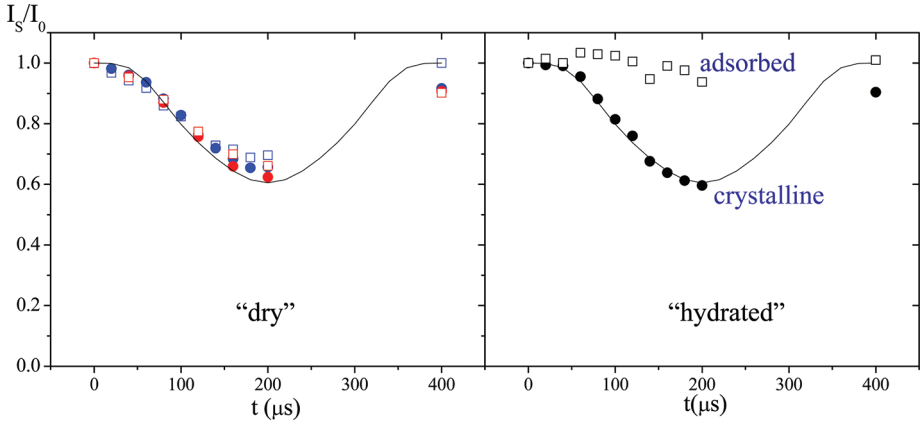

Figure 5. Experimental $^{15}N\{^{1}H\}$ SLF[PMLG5] dipolar evolution of the ^{15}N peak intensity for [1-^{13}C,^{15}N]glycine crystalline (solid symbols) and adsorbed (hollow symbols) onto SBA-15, at different temperatures (blue, −20 °C; black, 4 °C; red, 20 °C) as a function of homonuclear decoupling time *t*, at the "dry" state (left) and "hydrated" state (right). Simulations (curves) were calculated using N−H dipolar coupling of 11.4 kHz (1.01 Å for $-NH_3^+$) which is reduced by the C_3 rotation of $-NH_3^+$ and homonuclear dipolar decoupling scaling factor of 0.58. The adsorbed glycine peak at the "dry" state and at all temperatures gives rise to an evolution that closely overlaps that of the simulated curve of $-NH_3^+$; likewise, the crystalline peak regardless of hydration and temperature. At the "hydrated" state the adsorbed peak component is almost fully averaged.

the chemical shift alone cannot serve to identify the protonation state. The N−H dipolar evolution exposed by the SLF experiment for the adsorbed component of the ^{15}N peak (~5.1 ppm) in the "dry" state (Figure 5, left; hollow shapes) and independent of the hydration state for the crystalline component (7.7 ppm; Figure 5, solid shapes) overlaps the characteristic (calculated and model compounds[33] $-NH_3^+$ dipolar evolution curve (Figure 5, curves). This indicates that the surface adsorbed glycine molecules possess the protonated charged ammonium group, $-NH_3^+$, and it is this group that interacts with the surface silica sites.

The accumulated evidence of the glycine/SBA-15 interaction describes binding of the charged ammonium group at a specific surface site; this specific binding site consists of 3−4 silanol groups (Q^3) with well-defined geometry whose respective silicons are ~5 Å apart. All binding characteristics of glycine as identified above are similar to those reported earlier for alanine[33] when bound to the same SBA-15 silica surfaces. This similarity suggests that we evidence a repetitive binding pattern

dx.doi.org/10.1021/jp302431t | J. Phys. Chem. C 2012, 116, 9691−9702

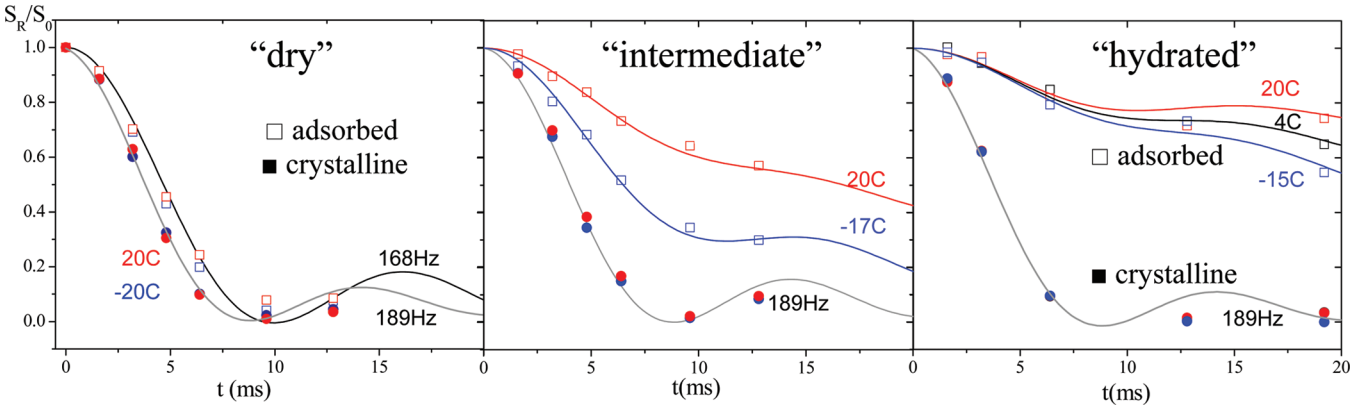

Figure 6. Experimental $^{15}N\{^{13}C\}$ S_R/S_0 REDOR evolution of [1-^{13}C,^{15}N]glycine/SBA-15 of the crystalline peak (solid symbols) and adsorbed peak (hollow) for the three hydration states, (a) "dry", (b) "intermediate" (middle), and (c) "hydrated" (right) states, at different temperatures (blue, −20 °C; black, 4 °C; red, 20 °C). Curves represent REDOR simulations that best fit the experimental data. The gray curve that best fits the crystalline peak regardless of hydration state, and temperature was calculated for dipolar $^{15}N\cdots^{13}C$ couplings of 189 Hz (2.54 Å) and was further apodized with an exponential, T_2-like, decay of 30 ms (10.67 Hz line broadening). The curve that fits the REDOR data of the adsorbed peak at the dry state was generated by a single REDOR evolution (168 Hz); the curves that fit the "intermediate" and "hydrated" states were obtained by a weighted summation of three calculated REDOR dipolar evolutions, each weight representing a population of glycine molecules as detailed in Tables 2 and 3.

of interacting moieties and specificity of binding site geometry and stoichiometry. In this scheme the positively charged amino groups facilitate the dominant binding interactions, while the negatively charged moieties, the carboxylates, have a minor role.

Dynamic Behavior of Adsorbed Glycine and Onset of Dissolution. *"Dry" State: Single Bound Population.* In order to characterize the dynamic behavior of surface adsorbed glycine, we take advantage of the intramolecular $^{15}N\cdots^{13}C_1$ dipolar coupling in [1-^{13}C,^{15}N]glycine. Its fixed internuclear $^{15}N\cdots^{13}C_1$ distance[65] of 2.49 Å translates to a measurable dipolar coupling strength of 189 Hz (accounting for small amplitude librations).[66] The calculated REDOR S_R/S_0 evolution for this coupling strength is exhibited by the continuous gray curve(s) in Figure 6 and is overlapped by the measured $^{15}N\{^{13}C\}$ REDOR data (filled shapes) of the crystalline glycine at the three hydration states (dry, intermediate, and hydrated) and across the −20 to +20 °C temperature range. The crystalline glycine $^{15}N\{^{13}C\}$ REDOR evolution, not being affected by increase of hydration and/or temperature, attest for the rigid character within the surface-induced polymorphs of glycine, being indistinguishable from regular molecular crystals of glycine.[67] At the same time, this rigid REDOR evolution serves as an internal static reference for the characterization of the surface-adsorbed glycine.

The measured $^{15}N\{^{13}C\}$ REDOR data of the adsorbed glycine at the "dry" state(Figure 6, left) show slower decay best fit by a REDOR curve of 168 Hz coupling strength. This 12% reduction compared to the static ("crystalline") dipolar coupling is interpreted in terms of averaging of the $^{15}N\cdots^{13}C_1$ dipolar interaction via fast, small amplitude, anisotropic molecular motion of the intramolecular $^{15}N\cdots^{13}C_1$ vector. Since the surface-bound glycine molecules are anchored via their ammonium group, the only motion possible is a small amplitude reorientation of the $^{15}N\cdots^{13}C_1$ vector such that its amine is fixed at the surface and the carboxylate is the pendent end which spans the motion. The $^{15}N\{^{13}C\}$ REDOR evolution at the "dry" state is independent of temperature between 4C and 20 °C, which further supports viewing glycine binding as stable and relatively rigid.

The physical picture that emerges from the accumulated data of the adsorbed glycine at the lowest hydration state is that of a *single population* of all likely bound glycine molecules, anchored to the silica surface via their positively charged ammonium moiety; simultaneously, the carboxylate end of the molecules undergoes fast, small amplitude motion. The ammonium moiety interacts with surface site consisting of 3−4 surface Si atoms. These observations attribute the glycine ammonium moiety the primary role in binding the silica surface, while the pendant carboxylate has small or no contribution.

Increased Hydration: Multiple Glycine Populations and Onset of Dissolution. The $^{15}N\{^{13}C\}$ REDOR evolution of the adsorbed glycine (5.1 ppm ^{15}N peak) changes dramatically upon hydration, at both the "intermediate" and "hydrated" states, and becomes temperature dependent (Figure 6, middle and right). The resulting REDOR evolution is much slower and levels off above zero and hence can no longer be fitted by a single dipolar coupling. In an attempt to fit the data and guided by our earlier study of alanine on SBA-15, we choose the presence of three populations with glycine undergoing different dynamics, each leading to a differently averaged dipolar interaction.[33] We also assume that all dynamic processes are at the fast limit relative to the inverse dipolar coupling strength (5 ms). Two populations with finite dipolar couplings and one with zero dipolar coupling (values shown in Tables 2 and 3) yield excellent fits to the experimental data (Figure 6, middle and right). The 168 Hz population is identical to that seen in the "dry" state, while the populations with farther averaged dipolar interactions (68 and 34 Hz for "intermediate" and "hydrated" states, respectively) represent glycine molecules undergoing rapid larger amplitude reorientation while anchored via their ammonium moiety as identified for alanine. A third population with averaged to zero dipolar coupling consists of

Table 2. $^{15}N\cdots^{13}C_1$ Dipolar Couplings and Populations at the Two Temperatures Obtained from Fitting the $^{15}N\{^{13}C\}$ REDOR Data for the Sample in the "Intermediate" State

	dipolar coupling (Hz)		
T (°C)	0	68	168
−17	15%	30%	55%
20	40%	35%	25%

dx.doi.org/10.1021/jp302431t | J. Phys. Chem. C 2012, 116, 9691−9702

Table 3. $^{15}N\cdots^{13}C_1$ Dipolar Couplings and Populations at the Three Temperatures Obtained from Fitting the $^{15}N\{^{13}C\}$ REDOR Data for the Sample in the "Hydrated" State

	dipolar coupling (Hz)		
T (°C)	0	34	168
−15	15%	65%	20%
4	40%	40%	20%
20	65%	15%	20%

dissolved glycine molecules that undergo rapid isotropic reorientation. A schematic representation of the three classes of dynamic states is shown in Figure 7 with the cones illustrating the reorientation boundaries (amplitude) of glycine when bound and the circle illustrating the isotropic motion.[69] These three dynamic classes that result upon surface hydration are interpreted in terms of surface binding sites accommodating water clusters of growing sizes.[36,37] The larger the cluster, the weaker is the binding potential and the larger is the reorientation amplitude spanned by the pendent carboxylate.

With increased hydration, as represented by the "intermediate" and "hydrated" states, the $^{15}N\{^{13}C\}$ REDOR evolution becomes strongly temperature dependent as seen in Figure 6. As anticipated, the distribution shifts toward the more mobile populations (Tables 2 and 3).

Interestingly, at the "hydrated" state the tightly bound population (20%) with 168 Hz dipolar coupling remains unchanged throughout the −15 to 20 °C temperature range. Redistribution occurs only between the "loosely" bound population to the dissolved (isotropic reorienting) population. This observation suggests that these 20% of the sites on the silica surface[42] have lower affinity to water, possibly arising from specific local geometry that cannot coaccommodate water molecules (at these low hydration levels).

Monitoring the N−H dipolar evolution (SLF[PMLG5] experiment) is an additional means to refine the characterization of the dynamics induced by the increased hydration. The adsorbed glycine component (^{15}N peak centered at ∼5.2 ppm) in the "hydrated" state at 4 °C (Figure 5, right; hollow shapes) shallows significantly, indicating almost fully averaged $N-H_3$ dipolar coupling. This almost vanished N−H dipolar coupling can arise from motional processes that are induced by the increased hydration. Two classes of such processes that will result in efficient averaging of the N−H dipolar coupling are possible: (i) onset of dissolution that leads to rapid isotropic reorientation and (ii) rapid hydrogen exchange between the anchored NH_3^+ group and adjacent water molecules and/or surface silanol hydroxyls. Recalling that at the "hydrated" state at 4 °C only about 40% undergo isotropic motion, while the remaining 60% are still anchored (Table 3); hence, the restricted reorientation of the latter cannot lead to the observed ($N-H_3$) averaging. We therefore conclude that the hydrogen exchange process between the ammonium of the surface-anchored glycine (the ∼40% with large amplitude reorientation) and the surrounding water and silanol hydroxyls is a pronounced process that contributes significantly to the observed averaging of the dipolar interaction. This process at increased hydration would eventually lead to dissolution and fully isotropic motion.

We also note that although the above dynamic processes lead to almost complete averaging of the $N-H_{(n)}$ dipolar coupling, the cross-polarization efficiency to ^{15}N is not suppressed, as would eventually occur at higher hydration states and faster dynamics.

Resolving the Different Hydrogen Environments. In order to obtain a more comprehensive insight into the glycine−silica interactions, a set of 2D $^1H\{^{29}Si/^{13}C/^{15}N\}$ HETCOR experiments was recorded for [1-^{13}C,^{15}N]glycine loaded SBA-15 at the "intermediate" hydration state (at room temperature). The resulting multinuclear 2D HETCOR spectra (Figure 8) enable to resolve the local hydrogen environments and identify hydrogen species which are not detectable in the 1D ^1H spectrum.

The $^1H\{^{29}Si\}$ 2D HETCOR spectrum shows cross-peaks of all three amorphous silica species (Q^2, Q^3, Q^4) with hydrogens at 3.3−3.7 ppm, assigned to silanol hydrogens (SiOH) and/or small clusters of water molecules.[36] The large ^1H cross-peak peak width across the different Si species reflects the highly heterogeneous hydrogen environments of the amorphous silica surface of SBA-15.

The $^1H\{^{13}C\}$ 2D HETCOR spectrum resolves the carboxylate cross-peaks of the two crystalline polymorphs and of the adsorbed glycine. Slices extracted from the 2D spectrum at the $^{13}COO^-$ chemical shift regions of the α and β polymorphs and of the absorbed glycine are shown as 1D ^1H spectra in Figure 9a,b,c, enabling better visualization of the enhanced resolution (see Table 1). The 1D spectra associated with the $^{13}COO^-$ resonance of the α and β glycine polymorphs reproduce the characteristic peak positions as in the ^1H spectra of the two neat polymorphs in accordance with literature data.[56] The adsorbed glycine 1D slice (a) shows a peak of the CH_2 hydrogens similar to β glycine, yet the $-NH_3^+$ peak shifts upfield by −0.8 to 7.2 ppm.

The $^{15}N\{^1H\}$ 2D HETCOR spectrum similarly resolves the ammonium cross-peaks of the crystalline and adsorbed glycine (Figure 8, right) with the extracted 1D slices shown in Figure

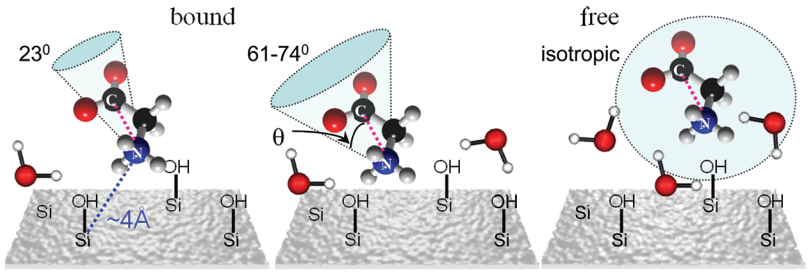

Figure 7. Schematic representation of the three distinct geometric-dynamic states of [1-^{13}C,^{15}N]glycine loaded onto SBA-15 at the "intermediate" and "hydrated" state. The left-most and center schematics represent bound, ammonium anchored glycine, with its carboxylate end undergoing rapid anisotropic reorientation spanning a cone whose head angle is determined from the extent dipolar coupling strengths (ν_{ave}/ν_{static}). The right-most graph represents onset of dissolution with glycine undergoing rapid isotropic reorientation.

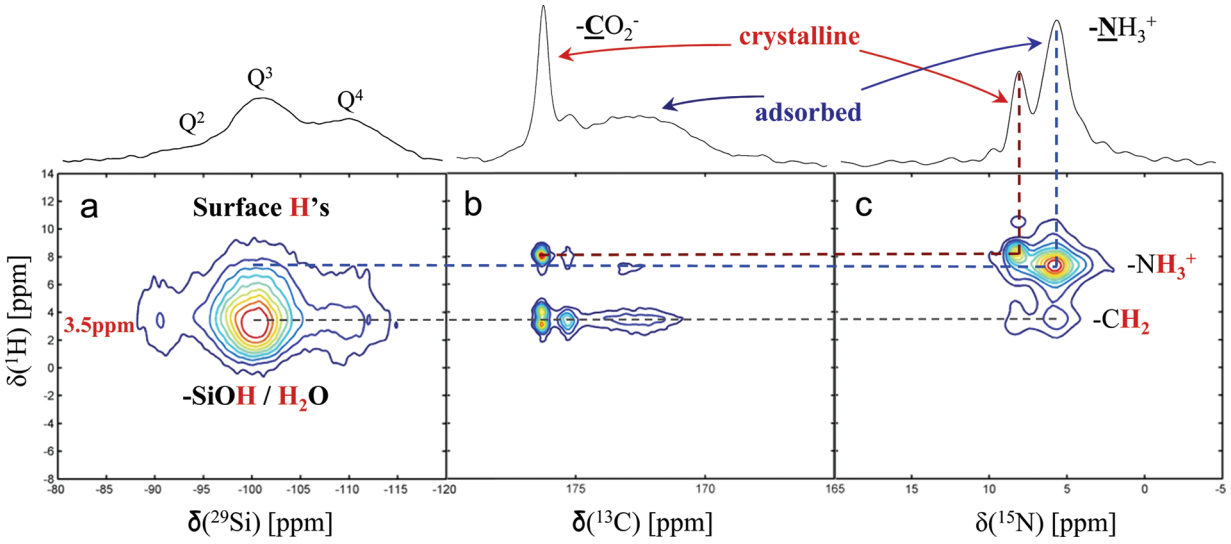

Figure 8. 2D HETCOR (wPMLG5) of [1-^{13}C,^{15}N]glycine loaded onto SBA-15 at the "intermediate" hydration state at room temperature: left, ^{1}H{^{29}Si} HETCOR 4 ms contact time; middle, ^{1}H{^{13}C} HETCOR 0.2 ms contact time; right, ^{1}H{^{15}N} HETCOR 0.3 ms contact time. Spinning speed of 10 kHz was employed.

9d,e. In the absence of polymorph resolution in the ^{15}N dimension the crystalline slice is a superposition of the b and c 1D slices, while the absorbed glycine slice shows peaks at the same positions as the adsorbed ^{1}H{^{13}C} slice (a) yet with opposite intensity ratios as expected.

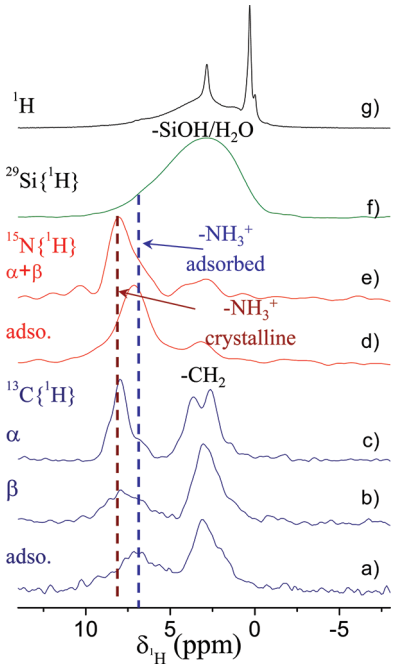

Figure 9. (a–f) 1D ^{1}H slices obtained from cross sections taken from the 2D ^{1}H{X} HETCOR spectra in Figure 8 of [1-^{13}C,^{15}N]glycine loaded onto SBA-15 at the "intermediate" hydration state. Each spectrum represents a summation through the chemical shift range surrounding the peak of interest as denoted in parentheses in the following. (a, b, c) ^{1}H slices from the ^{1}H{^{13}C} HETCOR ^{13}C of the α and β crystalline peaks and of the absorbed peak; (d, e) ^{1}H slices from the ^{1}H{^{15}N} HETCOR of the crystalline peak (α + β) and the absorbed peak, respectively, (f) full summation from the ^{1}H{^{29}Si} 2D HETCOR spectrum, and (g) ^{1}H 1D spectrum. Spinning speed of 10 kHz was employed throughout.

The 1D slice from the ^{1}H{^{29}Si} 2D HETCOR spectrum shown in Figure 9f exhibits for the most intense cross-peak of Q^3 an excessively broad peak reflecting the highly heterogeneous character of the hydrogens at the amorphous silica surface. Its close examination reveals a partially resolved shoulder centered at ~7.2 ppm, at the same chemical shift of $-NH_3^+$ hydrogens of adsorbed glycine (Figure 9a). This overlap between hydrogens of glycine ammonium and of a part of the Q^3 species correlates with the REDOR-identified glycine–surface interactions.

Noteworthy, the upfield shifts of the amine hydrogens (Figure 9) and ^{13}C-carboxylate and ^{15}N-ammonium groups of adsorbed glycine (Figure 1) relative to their crystalline chemical shifts are all attributed to the change of immediate chemical environment resulting from the interaction of glycine with the amorphous silica surface. However, these shifts alone cannot serve to infer which functional group is the one that directly interacts with the surface, a fact that is unambiguously unraveled only by the REDOR measurements.

Finally, the conventional ^{1}H MAS spectrum is shown for a reference in Figure 9g. The narrow peaks shown in this spectrum originate from the minute residual quantities of the pluronic P123 (EO20-PO70-EO20) used for the SBA-15 synthesis, yet not fully removed.[70] The combined three 2D HETCOR spectra, or alternatively their 1D slices, clearly show their inherent resolution and insight compared to the regular 1D spectrum.

CONCLUSIONS

Comprehensive chemical-structural-functional description of the binding mechanism glycine onto the high surface area mesoporous SBA-15 silica was achieved using solid-state NMR techniques. Primarily, tailoring dipole–dipole measurements enable the molecular level insight that was obscure and ambiguous to other experimental and computational attempts.

While the computational literature[38–40] emphasizes the higher reactivity of geminal silanols, Q^2's, vs Q^3 silanols and therefore directed efforts to compute possible interaction modes at Q^2 sites, the experimental studies clearly show the higher abundance and accessibility of the Q^3 silanol sites.[21,61,71]

dx.doi.org/10.1021/jp302431t | J. Phys. Chem. C 2012, 116, 9691–9702

Our study unequivocally demonstrates that the latter are the binding sites *de facto*. The interaction is shown to form between these surface silanols and glycine amine, the latter identified as the charged $-NH_3^+$ group ($^{15}N\{^1H\}$SLF NMR). Moreover, the geometry and stoichiometry of the intermolecular glycine-to-surface interaction are revealed by distance measurements ($^{29}Si\{^{15}N\}$ and $^{15}N\{^{29}Si\}$ REDOR NMR) between the $-NH_3^+$ and the surface Si species. The ammonium group is bound by 3−4 equidistant silanols, predominantly Q^3's, arranged in triangular or square geometry with Si···Si distances of ∼5 Å and with N···Si distances of 4.1 ± 0.3 Å. This geometric arrangement of the surface binding site is consistent with a group of vicinal silanols. The implication of the tight geometry of the ammonium with respect to the silanols is that the interaction cannot be mediated by water molecule(s) and is therefore classified as a direct interaction. While the $-NH_3^+$ group is surface anchored, the carboxylate end freely reorients with small amplitude (intramolecular $^{15}N\{^{13}C\}$REDOR NMR), indicating that this functional group has small or no contribution to surface binding. These observations are opposite to those predicted for glycine using DFT calculations[38−40] and as such further demonstrate the importance of direct experimental means to determine the molecular details of surface interactions.

Our study clearly shows the specific character of the surface binding sites, consisting of 3−4 hydroxyls of isolated silanols with a well-defined triangular or square geometry, these establish the binding potential of the charged ammonium, resulting in a tight, direct interaction. It should be emphasized that the forming sites do not resemble perfectly uniform, crystalline-like sites. These sites are highly heterogeneous as is reflected by the large peak widths of the binding silanols (^{29}Si NMR) and of the surface bound glycine (^{13}C and ^{15}N spectra). Earlier observations of narrow IR peaks of glycine's stretching modes led to conclude that the site is uniform and therefore specific.[38−40] The current NMR study shows clearly both the site specificity and its extensive heterogeneity, as expected on amorphous silica surface. This inherent heterogeneity does not allow the current data to delineate between the 3 or 4 surface site geometries.

The mechanism by which water molecules weaken the binding until onset of dissolution takes place is clearly exposed ($^{15}N\{^{13}C\}$REDOR NMR) upon increasing the hydration level. As water become more abundant, the reorientation amplitude of the carboxylate end is amplified and eventually becomes isotropic when the molecule is dissolved. In fact, upon hydration the emerging description is further refined by noting the coexistence of three distinct dynamic populations of glycine. The first population is that of the rigid molecules as in the single population of the driest hydration state: ammonium anchored with small reorientation amplitude of the pendent carboxylate end. The second population is of bound glycine, however, experiencing large-amplitude reorienting carboxylate. In the third population, glycine reorients isotropically, i.e., dissolved. This coexistence of distinct dynamic populations correlates with the simultaneous occurrence of different sizes of water clusters reported by Vega and coworkers;[36] the size of the water cluster which surrounds the adsorption site of glycine directly affects the binding potential and the resulting dynamics. We also note that once hydrated, although minutely (2−3 H_2O/nm^2), binding becomes temperature sensitive: increasing the temperature promotes dynamics and increases the more dynamic glycine populations in an equivalent manner to farther increased hydration. This is in contrast to the temperature independent binding at the "dry" state: in the absence of water molecules, binding is tight and relatively rigid (small reorientation amplitude). At increased hydration, additional to the reorientation motion of the pendent carboxylate, hydrogen exchange between bound glycine ammonium and the adjacent hydroxyls and/or water molecules takes place ($^{15}N\{^1H\}$SLF NMR). As these processes amplify they both lead to dissolution of glycine.

All the above identified binding characteristics of glycine are similar to those we have reported for alanine[33] when bound to the same SBA-15 silica surfaces. This similarity of interactions and dynamic modes represents a pattern of interacting moieties and specificity of binding site geometry and stoichiometry, which are expected for other amino acids with nonpolar side chain.

Moreover, SBA-15 silica surface was found to induce crystallization of glycine from undersaturated solution. This process is in fact competitive vs the sparse binding of molecules to the surface. Two crystalline polymorphs, α and β, of glycine were identified by their characteristic ^{13}C chemical shifts and the $^{15}N\cdots^{13}C$ peak connectivities (2D HETCOR). $^{15}N\{^{13}C\}$ and $^{15}N\{^{29}Si\}$ REDOR NMR substantiate their immobile crystalline character which is indistinguishable from regular molecular crystals of glycine. Yet, identifying whether this surface-induced crystallization occurs within or external to the mesoporous silica channels, what are the dimensions of the formed crystals and what is the molecular mechanism that induces their crystallization and stabilization are deferred to future studies.

In addition, a multinuclear set of 2D HETCOR experiments ($^1H\{^{13}C/^{15}N/^{29}Si\}$) serves to resolve and identify the hydrogen environments of adsorbed glycine vs the significantly distinct environments of crystalline glycine.

Our measurements provide direct, comprehensive, molecular-level identification of the bioorganic−inorganic interface, showing the binding functional groups of the adsorbed amino acid and the silica surface, the geometric constraints, stoichiometry and dynamics, and expose the role of water molecules for binding and dissolution.

The molecular level elucidation of specific interfacial interactions and the effect of surrounding water molecules on the structural and dynamical state of the surface bound molecules are of prime scientific and technological importance. Herein, we accomplish these goals by tailoring solid-state NMR methodology to provide direct and quantitative experimental evidence. The resulting detailed molecular-functional view further demonstrates the importance of solid-state NMR methods in the wide field of surface science.

AUTHOR INFORMATION

Corresponding Author

*Tel 972-4-8292583; Fax 972-4-8295703; e-mail chrschm@tx.technion.ac.il.

Notes

The authors declare no competing financial interest.

ACKNOWLEDGMENTS

We thank Prof. Shimon Vega from Weizmann Institute of Science and Prof. Aharon Loewenstein from Technion for fruitful discussions. Mr. Pini Shekhter from Technion is acknowledged for his assistance during the initial stages of

the research. This research was supported by a Grant from the GIF, the German−Israeli Foundation for Scientific Research and Development (G-1042-76.5/2009). We acknowledge the partial financial support from the Russell Berrie Nanotechnology Institute.

REFERENCES

(1) Nakanishi, K.; Sakiyama, T.; Imamura, K. *J. Biosci. Bioeng.* **2001**, *91*, 233−244.
(2) Taguchi, A.; Schuth, F. *Microporous Mesoporous Mater.* **2005**, *77*, 1−45.
(3) Mann, S. In *Biomineralizatiom: Principles and Concepts in Bioinorganic Materials Chemistry*; Oxford University Press: New York, 2001.
(4) Jahren, A. H.; Skinner, H. C. W. In *Biogeochemistry*; Elsevier Science: Oxford, 2007; Vol. *8*, Chapter 4, pp 1−69.
(5) Lowenstam, H. A.; Weiner, S. In *On Biomineralization*; Oxford University Press: New York, 1989; 324 pp.
(6) Besteman, K.; Lee, J.; Wiertz, F. G. M.; Heering, H. A.; Dekker, C. *Nano Lett.* **2003**, *3*, 727−730.
(7) Hersel, U.; Dahmen, C.; Kessler, H. *Biomaterials* **2003**, *24*, 4385−4415.
(8) Rimola, A.; Tosoni, S.; Sodupe, M.; Ugliengo, P. *ChemPhysChem* **2006**, *7*, 157−163.
(9) Lambert, J. *Origins Life Evol. Biospheres* **2008**, *38*, 211−242.
(10) Giraldo, L. F.; López, B. L.; Pérez, L.; Urrego, S.; Sierra, L.; Mesa, M. *Macromol. Symp.* **2007**, *258*, 129−141.
(11) Clarson, S. *Silicon* **2010**, *2*, 105−107.
(12) Iler, R. K. In *The Chemistry of Silica: Solubility, Polymerization, Colloid and Surface Properties, and Biochemistry*; John Wiley & Sons: New York, 1979.
(13) Linssen, T.; Cassiers, K.; Cool, P.; Vansant, E. F. *Adv. Colloid Interface Sci.* **2003**, *103*, 121−147.
(14) Kresge, C. T.; Leonowicz, M. E.; Roth, W. J.; Vartuli, J. C.; Beck, J. S. *Nature* **1992**, *359*, 710−712.
(15) Zhao, D. Y.; Feng, J. L.; Huo, Q. S.; Melosh, N.; Fredrickson, G. H.; Chmelka, B. F.; Stucky, G. D. *Science* **1998**, *279*, 548−552.
(16) Edler, K. J.; Reynolds, P. A.; White, J. W.; Cookson, D. *J. Chem. Soc., Faraday Trans.* **1997**, *93*, 199−202.
(17) Solovyov, L. A.; Kirik, S. D.; Shmakov, A. N.; Romannikov, V. N. *Microporous Mesoporous Mater.* **2001**, *44*, 17−23.
(18) Sauer, J.; Marlow, F.; Schuth, F. *Phys. Chem. Chem. Phys.* **2001**, *3*, 5579−5584.
(19) Zhang, J. Y.; Luz, Z.; Goldfarb, D. *J. Phys. Chem. B* **1997**, *101*, 7087−7094.
(20) Ruthstein, S.; Schmidt, J.; Kesselman, E.; Talmon, Y.; Goldfarb, D. *J. Am. Chem. Soc.* **2006**, *128*, 3366−3374.
(21) Shenderovich, I. G.; Buntkowsky, G.; Schreiber, A.; Gedat, E.; Sharif, S.; Albrecht, J.; Golubev, N. S.; Findenegg, G. H.; Limbach, H. H. *J. Phys. Chem. B* **2003**, *107*, 11924−11939.
(22) Baccile, N.; Laurent, G.; Bonhomme, C.; Innocenzi, P.; Babonneau, F. *Chem. Mater.* **2007**, *19*, 1343−1354.
(23) Stievano, L.; Piao, L. Y.; Lopes, I.; Meng, M.; Costa, D.; Lambert, J. *Eur. J. Mineral.* **2007**, *19*, 321−331.
(24) Zhao, Y. L.; Kolppen, S.; Frauenheim, T. *J. Phys. Chem. C* **2011**, *115*, 9615−9621.
(25) Pizzanelli, S.; Kababya, S.; Frydman, V.; Landau, M.; Vega, S. *J. Phys. Chem. B* **2005**, *109*, 8029−8039.
(26) Gibson, J. M.; Popham, J. M.; Raghunathan, V.; Stayton, P. S.; Drobny, G. P. *J. Am. Chem. Soc.* **2006**, *128*, 5364−5370.
(27) Gibson, J. M.; Raghunathan, V.; Popham, J. M.; Stayton, P. S.; Drobny, G. P. *J. Am. Chem. Soc.* **2005**, *127*, 9350−9351.
(28) Shaw, W. J.; Long, J. R.; Campbell, A. A.; Stayton, P. S.; Drobny, G. P. *J. Am. Chem. Soc.* **2000**, *122*, 7118−7119.
(29) Jaeger, C.; Groom, N.; S. Bowe, E.; Horner, A.; Davies, M. E.; Murray, R. C.; Duer, M. J. *Chem. Mater.* **2005**, *17*, 3059−3061.
(30) Maltsev, S.; Duer, M. J.; Murray, R. C.; Jaeger, C. *J. Mater. Sci.* **2007**, *42*, 8804−8810.
(31) Gullion, T.; Schaefer, J. *J. Magn. Reson.* **1989**, *81*, 196−200.
(32) Kaustov, L.; Kababya, S.; Belakhov, V.; Baasov, T.; Shoham, Y.; Schmidt, A. *J. Am. Chem. Soc.* **2003**, *125*, 4662−4669.
(33) Ben Shir, I.; Kababya, S.; Amitay-Rosen, T.; Balazs, Y. S.; Schmidt, A. *J. Phys. Chem. B* **2010**, *114*, 5989−5996.
(34) Steigel, A. In *Dynamic NMR Spectroscopy*; Spiess, H. W., Ed.; Springer-Verlag: Berlin, 1978.
(35) Goetz, J. M.; Schaefer, J. *J. Magn. Reson.* **1997**, *127*, 147−154.
(36) Amitay-Rosen, T.; Kababya, S.; Vega, S. *J. Phys. Chem. B* **2009**, *113*, 6267−6282.
(37) Grunberg, B.; Emmler, T.; Gedat, E.; Shenderovich, J.; Findenegg, G. H.; Limbach, H. H.; Buntkowsky, G. *Chem.—Eur. J.* **2004**, *10*, 5689−5696.
(38) Lomenech, C.; Bery, G.; Costa, D.; Stievano, L.; Lambert, J. F. *ChemPhysChem* **2005**, *6*, 1061−1070.
(39) Costa, D.; Lomenech, C.; Meng, M.; Stievano, L.; Lambert, J. F. *J. Mol. Struct.: THEOCHEM* **2007**, *806*, 253−259.
(40) Costa, D.; Tougerti, A.; Tielens, F.; Gervais, C.; Stievano, L.; Lambert, J. F. *Phys. Chem. Chem. Phys.* **2008**, *10*, 6360−6368.
(41) Meng, M.; Stievano, L.; Lambert, J. *Langmuir* **2004**, *20*, 914−923.
(42) Lopes, I.; Piao, L.; Stievano, L.; Lambert, J. *J. Phys. Chem. C* **2009**, *113*, 18163−18172.
(43) Gullion, T.; Schaefer, J. *Adv. Magn. Opt. Reson.* **1989**, *13*, 57.
(44) Veshtort, M.; Griffin, R. G. *J. Magn. Reson.* **2006**, *178*, 248−282.
(45) Massiot, D.; Fayon, F.; Capron, M.; King, I.; Calvé, S. L.; Alonso, B.; Durand, J.; Bujoli, B.; Gan, Z.; Hoatson, G. *Magn. Reson. Chem.* **2002**, *40*, 70−76.
(46) Vinogradov, E.; Madhu, P. K.; Vega, S. *Chem. Phys. Lett.* **1999**, *314*, 443−450.
(47) Vinogradov, E.; Madhu, P. K.; Vega, S. *J. Chem. Phys.* **2001**, *115*, 8983−9000.
(48) Vinogradov, E.; Madhu, P. K.; Vega, S. *Chem. Phys. Lett.* **2002**, *354*, 193−202.
(49) Leskes, M.; Madhu, P. K.; Vega, S. *Chem. Phys. Lett.* **2007**, *447*, 370−374.
(50) Leskes, M.; Madhu, P. K.; Vega, S. *J. Chem. Phys.* **2006**, 125.
(51) deAzevedo, E. R.; Saalwachter, K.; Pascui, O.; de Souza, A. A.; Bonagamba, T. J.; Reichert, D. *J. Chem. Phys.* **2008**, *128*, 104505.
(52) Fyfe, C. A.; Mueller, K. T.; Grondey, H.; Wongmoon, K. C. *Chem. Phys. Lett.* **1992**, *199*, 198−204.
(53) Jaroniec, C. P.; Filip, C.; Griffin, R. G. *J. Am. Chem. Soc.* **2002**, *124*, 10728−10742.
(54) Jehle, S.; Falb, M.; Kirkpatrick, J. P.; Oschkinat, H.; van Rossum, B. J.; Althoff, G.; Carlomagno, T. *J. Am. Chem. Soc.* **2010**, *132*, 3842−3846.
(55) Akiva-Tal, A.; Kababya, S.; Balazs, Y. S.; Glazer, L.; Berman, A.; Sagi, A.; Schmidt, A. *Proc. Natl. Acad. Sci. U. S. A.* **2011**.
(56) Stievano, L.; Tielens, F.; Lopes, I.; Folliet, N.; Gervais, C.; Costa, D.; Lambert, J. *Cryst. Growth Des.* **2010**, *10*, 3657−3667.
(57) Kimura, H.; Nakamura, K.; Eguchi, A.; Sugisawa, H.; Deguchi, K.; Ebisawa, K.; Suzuki, E.; Shoji, A. *J. Mol. Struct.* **1998**, *447*, 247−255.
(58) Yamauchi, K.; Kuroki, S.; Fujii, K.; Ando, I. *Chem. Phys. Lett.* **2000**, *324*, 435−439.
(59) Boldyreva, E.; Drebushchak, V.; Drebushchak, T.; Paukov, I.; Kovalevskaya, Y.; Shutova, E. *J. Therm. Anal. Calorim.* **2003**, *73*, 409−418.
(60) Chuang, I. S.; Maciel, G. E. *J. Phys. Chem. B* **1997**, *101*, 3052−3064.
(61) Shenderovich, I. G.; Mauder, D.; Akcakayiran, D.; Buntkowsky, G.; Limbach, H. H.; Findenegg, G. H. *J. Phys. Chem. B* **2007**, *111*, 12088−12096.
(62) Toke, O.; Cegelski, L. In *REDOR Applications in Biology: An Overview*; Encyclopedia of Magnetic Resonance; John Wiley & Sons, Ltd: New York, 2007; 1996.
(63) Peacor, D. R. *Z. Kristallogr.* **1973**, *138*, 274−298.
(64) Kobayashi, T.; DiVerdi, J. A.; Maciel, G. E. *J. Phys. Chem. C* **2008**, *112*, 4315−4326.

(65) Legros, J.-P.; Kvick, Å *Acta Crystallogr., Sect. B* **1980**, *36*, 3052−3059.
(66) The actual static dipolar coupling strength is 198 Hz; reduced dipolar coupling strength of 189 Hz was measured for molecular crystals of glycine by $^{15}N\{^{13}C\}$ REDOR[31] and was attributed to small amplitude librations.[67] Our $^{15}N\{^{13}C\}$ REDOR evolution measured for Gly/SBA-15 at the three hydration states are best fit[44] by the static literature value[68] of 189 Hz after apodization with a T_2 exponential decay of 30 ms. Because of the relatively small intensity of the β polymorph peak, the analysis was done referring to both α and β as a single peak.
(67) Goetz, J. M.; Schaefer, J. *J. Magn. Reson.* **1997**, *129*, 222−223.
(68) Jaroniec, C. P.; Tounge, B. A.; Rienstra, C. M.; Herzfeld, J.; Griffin, R. G. *J. Magn. Reson.* **2000**, *146*, 132−139.
(69) The averaging of the dipolar coupling reflects reorientation of the vector connecting the amine nitrogen and the carboxylate carbon; the extent of averaging, ν_{Ave}/ν_D, serves to estimate the range of orientations, 0 to θ, that are uniformly spanned by this vector using the relation $\langle(3\cos^2\theta - 1)/2\rangle$ (Vega, S.; private communication); the different coupling strengths (Tables 2 and 3) of 168, 68−34, and 0 Hz imply the respective θ angles of 23°, 61°−74°, and isotropic.
(70) Bae, Y. K.; Han, O. H. *Microporous Mesoporous Mater.* **2007**, *106*, 304−307.
(71) Buntkowsky, G.; Breitzke, H.; Adamezyk, A.; Roelofs, F.; Emmler, T.; Gedat, E.; Grunberg, B.; Xu, Y.; Limbach, H. H.; Shenderovich, J.; Vyalikh, A.; Findenegg, G. *Phys. Chem. Chem. Phys.* **2007**, *9*, 4843−4853.